PHYSICAL REVIEW B **108**, 195429 (2023)

Valley polarization and stable triplet exciton formation in two-dimensional lateral heterostructure of kagome *h*-BN and graphene

Souren Adhikary,[1] Sasmita Mohakud,[2] and Sudipta Dutta[1,*]
[1]*Department of Physics, Indian Institute of Science Education and Research (IISER) Tirupati, Tirupati 517507, Andhra Pradesh, India*
[2]*Department of Physics, School of Advanced Sciences, Vellore Institute of Technology, Vellore, Tamil Nadu 632014, India*

(Received 14 August 2023; revised 1 November 2023; accepted 1 November 2023; published 21 November 2023)

Broken spatial inversion symmetry in semiconducting materials with time-reversal pair valleys can exhibit valley polarization. Based on first-principles calculations, here we propose a lateral heterostructure of a kagome lattice of *h*-BN and hexagonal graphene domains that exhibits opposite Berry curvature in inequivalent **K** and **K**′ valleys. Explicit consideration of the excitonic scattering processes within the *GW* and Bethe-Salpeter equation formalism confirm insignificant intervalley coupling and consequent valley-polarization ability along with a 0.46 eV higher binding energy of triplet excitons. Such a heterostructure with a large charge carrier mobility can be exploited for advanced valleytronic and optoelectronic applications.

DOI: 10.1103/PhysRevB.108.195429

I. INTRODUCTION

The quantum degrees of freedom of electrons can serve as the foundations for information storage and processing [1]. Two-dimensional (2D) hexagonal materials with broken spatial inversion symmetry possess an additional electronic degree of freedom known as the valley, alongside their charge and spin [2,3]. The primary challenge in harnessing the valley degree of freedom lies in overcoming the valley degeneracy [4,5]. Significant efforts have been dedicated to achieve valley polarization, either through intrinsic mechanisms or by employing extrinsic strategies [6–9]. For example, the inherent broken inversion symmetry in monolayer transition metal dichalcogenide systems leads to opposite Berry curvature at the **K** and **K**′ valleys in momentum space [10–12]. Consequently, the electrons in these two valleys selectively couple with opposite helicity of circularly polarized light to form excitons [12]. When a transverse electric field is applied to the system, the movement of charge carriers in the **K** and **K**′ valleys occurs in opposite directions. These carriers can act as the exciton qubits that are capable of storing information as "zero" and "one" [13]. Extrinsically, the valley degeneracy can be lifted through applied magnetic fields by a few meV [6,7,14].

Graphene, the most widely studied 2D system, lacks any gap at the valleys and preserves the spatial inversion symmetry that results in zero Berry curvature [15,16]. Creating a staggered sublattice potential can serve as a way to break the inversion symmetry [10]. In this regard, 2D hexagonal boron nitride (*h*-BN) could act as an ideal candidate for showcasing valley-related properties [17,18]. However, due to its weak screening and large insulating gap, the excitons in two valleys couple with each other [19]. Such intervalley coupling significantly suppresses the valley-polarization ability of *h*-BN. Therefore, the manipulation of spatial inversion symmetry and intervalley scattering in 2D materials are critical steps towards unlocking their potential applications in valley-based information storage.

Controlled modifications of lattice structures can induce such functionalities in experimentally conducive 2D materials. Recently, a 2D kagome lattice comprising polymerized heterotriangulene units has been shown computationally to exhibit unique electronic behavior, featuring a Dirac band enclosed by two flat bands, that can be further engineered to obtain semimetallic or semiconducting properties [20]. These 2D kagome covalent organic frameworks have been successfully synthesized on the Au(111) surface [21,22]. Such a kagome lattice based on graphene has been predicted to show opposite spin localization in adjacent triangulene units, thereby breaking the spatial inversion symmetry [23]. A subsequent gap opening at the two valleys ensures its valley-polarization ability within first-principles and mean-field level of calculations [23].

In this paper, we construct a kagome lattice of *h*-BN with a subsequent filling of the hexagonal voids by graphene domains to form their lateral heterostructure. This system preserves the time-reversal symmetry with a moderate band gap at the two valleys and breaks the spatial inversion symmetry. Consequently, this system exhibits opposite Berry curvatures at the two valleys with minimal intervalley scattering that are confirmed within density functional theory (DFT) along with the *GW* and Bethe-Salpeter equation (BSE) approximation. The computational details are provided in the Supplemental Material (SM) [24] (see also Refs. [25–34] therein). This system also shows a higher stabilization of the triplet excitons over a singlet that can be exploited for the enhancement of the quantum efficiency for optoelectronic applications.

II. RESULTS AND DISCUSSION

First, we construct a kagome lattice of *h*-BN, cutting it out from its monolayer and name it hBNK. We passivate the edges by hydrogen atoms to eliminate the dangling bonds to

---

[*] sdutta@iisertirupati.ac.in

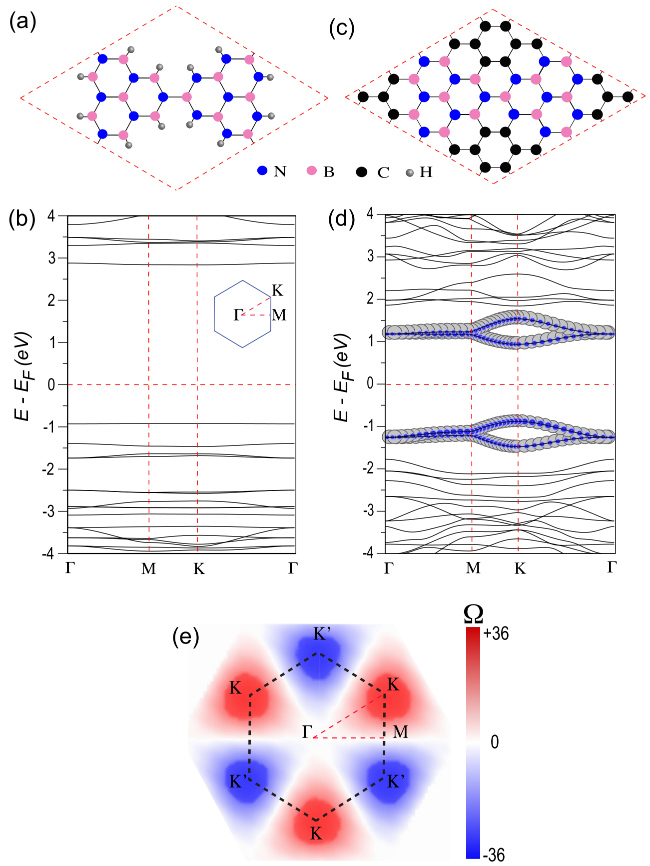

FIG. 1. (a) The rhombus unit cell of hBNK lattice along with its (b) electronic band structure. The vertical dashed lines indicate high-symmetric points in the hexagonal BZ, shown in the inset. (c) The rhombus unit cell of the lateral heterostructure hBNK-G along with its (d) electronic band structure. The contribution of all carbon atoms and all boron plus nitrogen atoms in the frontier bands are shown as gray and blue (dark) circles, respectively. Both the band structures are obtained within the PBE approximation and scaled with respect to the Fermi energy (horizontal dashed lines). (e) The Berry curvature (in atomic units) of the topmost valence band of hBNK-G over the hexagonal first BZ (dashed hexagon).

avoid any edge reconstruction. The unit cell of the system in a nonmagnetic ground state with a lattice constant of 12.67 Å is shown in Fig. 1(a). The electronic band dispersions of hBNK, as obtained within the generalized gradient approximation with the Perdew-Burke-Ernzerhof (PBE) exchange and correlation functional, are shown in Fig. 1(b). The band gap of 4.7 eV in monolayer *h*-BN [19] significantly reduces to 3.76 eV upon construction of the kagome lattice. The bands around the Fermi energy becomes dispersionless, owing to the enhanced electronic localization in the presence of hexagonal voids in the lattice. As a result, the charge carrier mobility of hBNK is expected to be very low and may find limited applications in semiconductor devices. Furthermore, these bands can induce enhanced intervalley coupling as has been seen in the case of monolayer *h*-BN. The less dispersive bands from the Γ to **M** high-symmetry direction in *h*-BN leads to intervalley coupling and suppresses its valley-polarization ability [19].

However, such dispersionless bands can be tuned by filling up the hexagonal voids by graphene domains, as shown in Fig. 1(c) and in Fig. S1 [24]. We refer to this system as hBNK-G that shows a nonmagnetic ground state with an optimized lattice constant of 12.49 Å. The minimal lattice mismatch between graphene and *h*-BN allows the seamless formation of such a lateral heterostructure with precise control over the domain shape and sizes, as evident from earlier experimental reports [35–37]. Any edge disorder in hBNK can be avoided by the formation of such a heterostructure and that in turn alters the energy dispersion significantly, as can be seen in Fig. 1(d). Further analysis based on cohesive energy and *ab initio* molecular dynamics (AIMD) calculations proves the stability of such a lateral heterostructure even at room temperature [24]. The hBNK-G system now shows dispersive bands near the Fermi energy with a significant reduction of the band gap to 1.82 eV at the high-symmetry point **K**, that enables the system for visible spectrum absorption. This substantial change in the energy dispersions can be attributed to the presence of graphene domains that play a dominant role via significant hybridization with the hBNK lattice. This is evident from the projected band structure of hBNK-G in Fig. 1(d). The frontier bands show minor contributions from combined B and N atoms and major contributions from C atoms. The enhanced dispersion results in a high charge carrier mobility of 1.4×10^3 cm^2 V^{-1} s^{-1} in hBNK-G [24], which is comparable with that of black phosphorene [38]. Therefore, by creating such a lateral heterostructure, one can enhance the optical and semiconducting properties.

Furthermore, such an enhanced dispersion along with the formation of valleys at the time-reversal pair of high-symmetric points **K** and **K**′ in the first Brillouin zone (BZ) can lead to efficient valley polarization in hBNK-G, owing to its broken spatial inversion symmetry, as can be seen in Fig. 1(c). This can lead to circular dichroism properties in this system as well. To explore it further, we calculate the Berry curvature for the valence band of hBNK-G using the DFT-based tight-binding Hamiltonian and Wannier functions as follows [39],

$$\Omega(\mathbf{k}) = -\sum_{n\neq n'} \frac{2\,\mathrm{Im}\langle\psi_{n\mathbf{k}}|v_x|\psi_{n'\mathbf{k}}\rangle\langle\psi_{n'\mathbf{k}}|v_y|\psi_{n\mathbf{k}}\rangle}{(\varepsilon_n-\varepsilon_{n'})^2}, \tag{1}$$

where the summation is over all the occupied valence bands, $v_{x(y)}$ is the velocity operator along the $x(y)$ direction, and ε_n is the nth eigenstate energy. From Fig. 1(e), it can be seen that the Berry curvature has an opposite sign with the same magnitude at the two valleys, **K** and **K**′. This leads to an optical selection rule that dictates selective excitations at the two valleys under the irradiation of circularly polarized light of different polarities. Moreover, since the Berry curvature behaves analogously to the magnetic field in the momentum space, an in-plane electric field generates drift velocities of similar charge carriers, i.e., electrons or holes in the opposite directions due to a Lorentz-like force. This can be exploited to realize a valley-Hall effect in hBNK-G. Note that the magnitude of the Berry curvature at two valleys comes out to be 36 in bohr^2 [24], which is an order of magnitude higher than that of the superatomic graphene lattice reported earlier

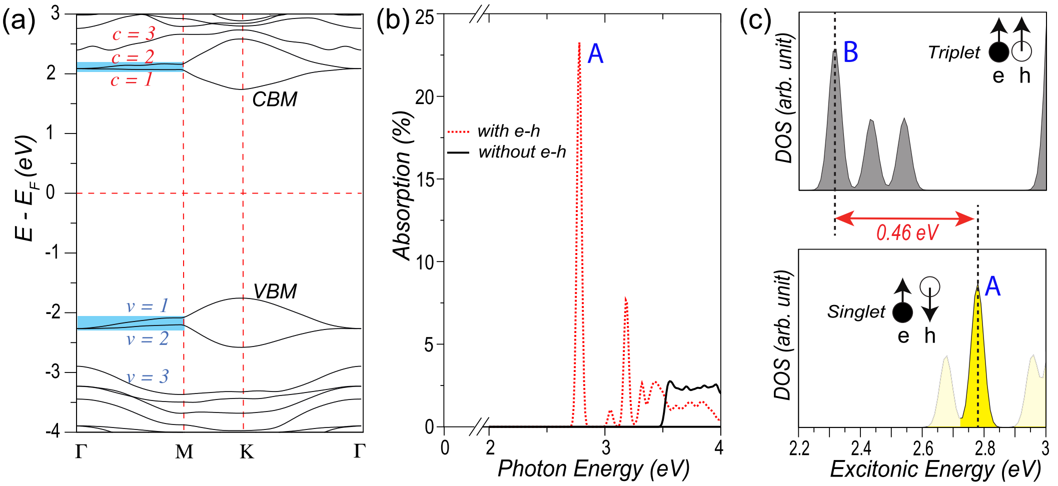

FIG. 2. (a) The *GW* band structure of hBNK-G. The band structure is scaled with respect to the Fermi energy (horizontal dashed line). The valence (v) and conduction bands (c) are marked with numerical values, starting from the frontier bands, denoted by valence band maxima (VBM) and conduction band minima (CBM). The nondispersive nature of the bands v (c) = 1 and 2 over the Γ to **M** point in the first BZ is highlighted with shaded rectangles. (b) The optical absorption spectra of hBNK-G, as obtained with (dotted line) and without (solid line) quasielectron and quasihole interactions. A constant broadening of 20 meV is considered here. The first bright singlet exciton peak is marked with *A*. (c) The DOS of triplet (upper panel) and singlet (lower panel) excitons of the same system. The DOS corresponding to the dark singlets are masked. The gap between the first triplet exciton (*B*) and first bright singlet exciton (*A*) is shown by a double-headed arrow.

[23] and comparable to the transition metal dichalcogenide systems [40].

However, the quasiparticle nature of the excitons and their intervalley scattering can substantially suppress the valley-polarization ability, as has been observed in the case of a 2D *h*-BN system [19]. Due to reduced Coulomb screening in 2D, such scattering processes play a dominant role and require a many-body treatment [41]. This has driven us to first investigate the quasiparticle dispersion within the *GW* approximation [42] that leads to the following eigenvalue equation,

$$\left[-\tfrac{1}{2}\nabla^2 + V_{\text{ext}} + V_H + \Sigma\left(\epsilon_{n\mathbf{k}}^{\text{QP}}\right)\right]\psi_{n\mathbf{k}}^{\text{QP}} = \epsilon_{n\mathbf{k}}^{\text{QP}}\psi_{n\mathbf{k}}^{\text{QP}}, \tag{2}$$

where Σ is the self-energy operator within the *GW* approximation and $\epsilon_{n\mathbf{k}}^{\text{QP}}$ and $\psi_{n\mathbf{k}}^{\text{QP}}$ are the quasiparticle energies and wave functions, respectively. The term V_{ext} is the potential energy due to the ion-electron interactions and V_H is the Hartree energy. The electronic self-energy correction results in an enhanced quasiparticle gap of 3.5 eV at the valleys, as can be seen in Fig. 2(a). An additional self-consistent update for G, i.e., G_1W_0, results in the same gap. The self-energy correction is highest at the Γ point with 1.89 eV and lowest at the **K** point with 1.67 eV, whereas the correction at the **M** point is 1.86 eV.

We further explore the excitonic wave functions within BSE formalism [43] using the following equation,

$$\left(\epsilon_{c\mathbf{k}}^{\text{QP}} - \epsilon_{v\mathbf{k}}^{\text{QP}}\right)A_{vc\mathbf{k}}^{S} + \sum_{v'c'\mathbf{k}'}\langle vc\mathbf{k}|K^{eh}|v'c'\mathbf{k}'\rangle = \Omega^{S}A_{vc\mathbf{k}}^{S}, \tag{3}$$

where v (c) represents the valence (conduction) band index, $A_{vc\mathbf{k}}^{S}$ is the envelope function of the exciton, Ω^S is the excitation energy of the exciton state $|S\rangle$, and K_{eh} is the electron-hole interaction kernel. Using the solution of the above equation, the absorption spectra are obtained from the imaginary part of the dielectric function $\varepsilon_2(\omega)$,

$$\varepsilon_2(\omega) = \frac{16\pi^2 e^2}{\omega^2}\sum_{S}|\mathbf{P}\cdot\langle 0|\mathbf{v}|S\rangle|^2\delta(\omega - \Omega^S), \tag{4}$$

where $\mathbf{P}$ is the polarization of the incoming photon, e is the electronic charge, $\mathbf{v}$ is the velocity operator, $\langle 0|$ is the Fock space within the DFT level, and $|S\rangle$ is the excitonic wave function. The convergence parameters of BSE calculations are provided in the SM [24].

We calculate the absorption spectra of hBNK-G in the presence of linearly polarized light, considering three valence and four conduction bands to attain the convergence and plot the same in Fig. 2(b). The formation of a bright singlet exciton peak *A* at 2.78 eV indicates a large excitonic binding energy of 0.72 eV with respect to the quasiparticle gap. The excitonic eigenvalue analysis shows that this peak arises from two degenerate excitonic states (see Fig. S5 [24]). This degeneracy can be broken by probing the circularly polarized light of the defined chirality. We further plot the density of states (DOS) corresponding to the singlet and triplet excitons in Fig. 2(c), which reveals a large singlet-triplet gap of 0.46 eV with a more stable triplet exciton. Note that, below the DOS corresponding to the bright singlet exciton peak *A*, there appears a dark singlet exciton, characterized by negligible oscillator strength as compared to the bright one. That is why the singlet-triplet splitting is calculated with respect to the bright singlet exciton, i.e., peak *A*.

To investigate this large splitting, we explore the optical transitions among a few valence and conduction bands that are marked with numerical indices in Fig. 2(a). We calculate the total excitation amplitude in between two band indices using the equation $W_{\text{tot}} = \sum_{\mathbf{k}}|A_{vc\mathbf{k}}|^2$, where $A_{vc\mathbf{k}}$ is the amplitude of the particular excitation. We present the corresponding data in Table I. We find that the singlet excitons get formed mostly

TABLE I. The contributions (in %) from band-to-band optical transitions towards the formation of the first bright singlet (A) and first triplet (B) excitonic peaks. The values are rounded off up to the first order.

Singlet	$c = 1$	$c = 2$	$c = 3$	Triplet	$c = 1$	$c = 2$	$c = 3$
$v = 1$	97.9	0.5	0.1	$v = 1$	77.3	03.4	0.0
$v = 2$	00.4	0.4	0.1	$v = 2$	03.7	15.6	0.0
$v = 3$	00.2	0.1	0.1	$v = 3$	00.0	00.0	0.0

due to the transition from the top of the valence band ($v = 1$) to the bottom of the conduction band ($c = 1$). However, excitations among bands, $v = 1, 2$ and $c = 1, 2$ show substantial contributions towards the triplet exciton. To gain further insight, we investigate the **k**-resolved optical transitions for both the first bright singlet (peak A) and first triplet (peak B) excitons in terms of the **k**-resolved envelope function and plot $\sqrt{\sum_i |A_{\mathbf{k}}^{S_i}|^2}$ in Figs. 3(a) and 3(b), respectively. Note that here i is the degeneracy of the excitonic states. As can be seen, the singlet exciton is being formed due to the optical transitions at and near the **K** and **K**′ valleys [see Fig. 3(a)]. Significant contributions to the triplet excitons are arising from these valleys too [see Fig. 3(b)]. This can be attributed to the attractive direct electron-hole screened Coulomb interaction term in the interaction kernel, which contributes towards the formation of both singlet and triplet excitons [43]. Further investigation reveals that the triplet exciton formation at the valleys is a consequence of only $v = 1$ to $c = 1$ transitions [see Fig. 3(c)]. In addition to this, the optical transitions among the other bands towards the triplet formation happen mostly over the $\Gamma - \mathbf{M}$ path [see Fig. 3(d)], where these bands are mostly dispersionless, as highlighted in Fig. 2(a). Such flat-band-induced triplet exciton formation has been reported in a superatomic graphene lattice [44].

The envelope function plots in Figs. 3(a) and 3(b) further indicate the extent of intervalley coupling for singlet and triplet excitons, respectively. The triplet excitons experience strong intervalley scattering, as evident from the higher magnitude of the envelope function in between the two valleys. However, in the case of the bright singlet exciton, the intervalley coupling between the **K** and **K**′ valleys comes out to be only 12.5%. The higher magnitude of opposite Berry curvature at these two valleys and such minimal intervalley coupling indicates the efficient valley-polarization ability of the hBNK-G system. For further confirmation, we calculate the oscillator strengths of the bright singlet excitation under the irradiation of circularly polarized light of different chirality over the first BZ, using the following expression [11,19,45],

$$I^{\sigma^{\pm}} \sim \sum_i \left|A_{\mathbf{k}}^{S_i} \mathbf{P} \cdot \langle v\mathbf{k}|(v_x\hat{x} \pm i v_y\hat{y})|c\mathbf{k}\rangle\right|^2, \tag{5}$$

where $\sigma^{\pm}$ indicate different chiralities of the circularly polarized light, v_x (v_y) is the component of the velocity operator, and $\hat{x}$ ($\hat{y}$) is the unit vector along the x (y) direction. As mentioned before, the doubly degenerate eigenstates corresponding to the bright singlet exciton get split while interacting with the left (σ^+) and right (σ^-) circularly polarized light and we plot the corresponding oscillator strengths in Figs. 3(e) and 3(f), respectively. As can be seen, the σ^+ forms excitons selectively at the **K** valley. In the presence of an in-plane electric field, the electrons and holes in this valley will prefer to move in opposite directions, owing to opposite Berry curvatures of the valence and conduction bands. However, the combination of σ^- light with the in-plane electric field will drive the charge carriers at the **K**′ valley in opposite directions as compared to the other valley, owing to the sign reversal of the Berry curvature [see Fig. 1(e)]. Therefore, the hBNK-G system can exhibit an efficient circular dichroism valley-Hall effect.

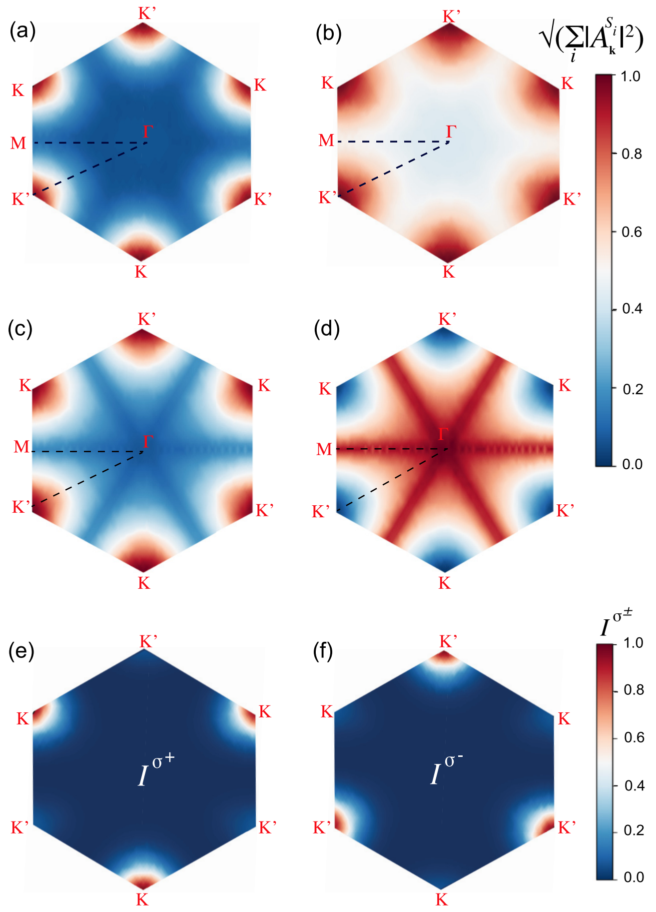

FIG. 3. The square root of the sum of the squared excitonic envelope function $A_{\mathbf{k}}^{S_i}$ of (a) the first bright singlet (A) and (b) the first triplet (B) exciton of hBNK-G over the hexagonal first BZ, as obtained with a converged number of bands consisting of three valence and four conduction bands. (c) The contribution towards the first triplet exciton from the band edges, i.e., one valence band (topmost) and one conduction band (bottommost). (d) The resultant values after subtracting the values of (c) from (b). Therefore, it represents the contribution towards the first triplet exciton from the other two valence and the other three conduction bands other than the band edges. The color bar displays the normalized value of the same. The oscillator strengths of the first bright singlet (A) exciton in the presence of (e) left- and (f) right-handed circularly polarized light. The color bar depicts the normalized values of the oscillator strength.

III. CONCLUSIONS

To summarize, based on first-principles calculations, we propose a 2D lateral heterostructure of a kagome lattice of *h*-BN and hexagonal graphene domains that can exhibit promising electronic and optical properties. An optical gap of 2.78 eV with 0.72 eV binding energy for singlet excitons and a high charge carrier mobility of 1.4×10^3 cm^2 V^{-1} s^{-1} indicates efficient optoelectronic properties of this hBNK-G system. Furthermore, this system is capable of stabilizing the triplet exciton over the singlet one by 0.46 eV that can enhance the exciton lifetime and the quantum efficiency of optical absorption [46,47]. Owing to its broken spatial inversion symmetry, this system exhibits opposite Berry curvature at the time-reversal pair valleys $\mathbf{K}$ and $\mathbf{K}'$ with negligible intervalley scattering that is confirmed within many-body BSE calculations. Consequently, the charge carriers at each valley can be excited selectively by controlling the chirality of the circularly polarized light, as shown explicitly in terms of their oscillator strengths. This property can be exploited for realizing excitonic qubits through a circular dichroism valley-Hall device. Our study shows different pathways of inducing interesting optical properties by constructing a kagome-based periodic lateral heterostructure of widely used 2D materials such as graphene and *h*-BN.

ACKNOWLEDGMENTS

S.A. and S.D. thank IISER Tirupati for Intramural Funding and Science and Engineering Research Board, Department of Science and Technology, Government of India for a research grant (CRG/2021/001731). The authors thank Prof. K. Wakabayashi (Kwansei Gakuin University) for illuminating discussions. The authors acknowledge National Supercomputing Mission (NSM) for providing computing resources of “PARAM Brahma” at IISER Pune, which is implemented by C-DAC and supported by the Ministry of Electronics and Information Technology (MeitY) and DST, Government of India.

---

[1] K. F. Mak, D. Xiao, and J. Shan, Light–valley interactions in 2D semiconductors, Nat. Photonics **12**, 451 (2018).

[2] K. F. Mak, K. L. McGill, J. Park, and P. L. McEuen, The valley Hall effect in MoS$_2$ transistors, Science **344**, 1489 (2014).

[3] S. Wu, J. S. Ross, G.-B. Liu, G. Aivazian, A. Jones, Z. Fei, W. Zhu, D. Xiao, W. Yao, D. Cobden *et al.*, Electrical tuning of valley magnetic moment through symmetry control in bilayer MoS$_2$, Nat. Phys. **9**, 149 (2013).

[4] Z. Ye, D. Sun, and T. F. Heinz, Optical manipulation of valley pseudospin, Nat. Phys. **13**, 26 (2017).

[5] H. Zeng, J. Dai, W. Yao, D. Xiao, and X. Cui, Valley polarization in MoS$_2$ monolayers by optical pumping, Nat. Nanotechnol. **7**, 490 (2012).

[6] G. Aivazian, Z. Gong, A. M. Jones, R.-L. Chu, J. Yan, D. G. Mandrus, C. Zhang, D. Cobden, W. Yao, and X. Xu, Magnetic control of valley pseudospin in monolayer WSe$_2$, Nat. Phys. **11**, 148 (2015).

[7] D. MacNeill, C. Heikes, K. F. Mak, Z. Anderson, A. Kormányos, V. Zólyomi, J. Park, and D. C. Ralph, Breaking of valley degeneracy by magnetic field in monolayer MoSe$_2$, Phys. Rev. Lett. **114**, 037401 (2015).

[8] L. Xu, M. Yang, L. Shen, J. Zhou, T. Zhu, and Y. P. Feng, Large valley splitting in monolayer WS$_2$ by proximity coupling to an insulating antiferromagnetic substrate, Phys. Rev. B **97**, 041405(R) (2018).

[9] T. Hu, G. Zhao, H. Gao, Y. Wu, J. Hong, A. Stroppa, and W. Ren, Manipulation of valley pseudospin in WSe$_2$/CrI$_3$ heterostructures by the magnetic proximity effect, Phys. Rev. B **101**, 125401 (2020).

[10] D. Xiao, W. Yao, and Q. Niu, Valley-contrasting physics in graphene: Magnetic moment and topological transport, Phys. Rev. Lett. **99**, 236809 (2007).

[11] D. Xiao, G.-B. Liu, W. Feng, X. Xu, and W. Yao, Coupled spin and valley physics in monolayers of MoS$_2$ and other group-VI dichalcogenides, Phys. Rev. Lett. **108**, 196802 (2012).

[12] T. Cao, G. Wang, W. Han, H. Ye, C. Zhu, J. Shi, Q. Niu, P. Tan, E. Wang, B. Liu *et al.*, Valley-selective circular dichroism of monolayer molybdenum disulphide, Nat. Commun. **3**, 887 (2012).

[13] G. Pacchioni, Valleytronics with a twist, Nat. Rev. Mater. **5**, 480 (2020).

[14] A. Srivastava, M. Sidler, A. V. Allain, D. S. Lembke, A. Kis, and A. Imamoğlu, Valley Zeeman effect in elementary optical excitations of monolayer WSe$_2$, Nat. Phys. **11**, 141 (2015).

[15] A. H. Castro Neto, F. Guinea, N. M. R. Peres, K. S. Novoselov, and A. K. Geim, The electronic properties of graphene, Rev. Mod. Phys. **81**, 109 (2009).

[16] A. K. Geim and K. S. Novoselov, The rise of graphene, Nat. Mater. **6**, 183 (2007).

[17] Z. Song, Z. Li, H. Wang, X. Bai, W. Wang, H. Du, S. Liu, C. Wang, J. Han, Y. Yang *et al.*, Valley pseudospin with a widely tunable bandgap in doped honeycomb BN monolayer, Nano Lett. **17**, 2079 (2017).

[18] C. Elias, P. Valvin, T. Pelini, A. Summerfield, C. Mellor, T. Cheng, L. Eaves, C. Foxon, P. Beton, S. Novikov *et al.*, Direct band-gap crossover in epitaxial monolayer boron nitride, Nat. Commun. **10**, 2639 (2019).

[19] F. Zhang, C. S. Ong, J. W. Ruan, M. Wu, X. Q. Shi, Z. K. Tang, and S. G. Louie, Intervalley excitonic hybridization, optical selection rules, and imperfect circular dichroism in monolayer h-BN, Phys. Rev. Lett. **128**, 047402 (2022).

[20] Y. Jing and T. Heine, Two-dimensional kagome lattices made of hetero triangulenes are Dirac semimetals or single-band semiconductors, J. Am. Chem. Soc. **141**, 743 (2019).

[21] N. Pavliček, A. Mistry, Z. Majzik, N. Moll, G. Meyer, D. J. Fox, and L. Gross, Synthesis and characterization of triangulene, Nat. Nanotechnol. **12**, 308 (2017).

[22] G. Galeotti, F. De Marchi, E. Hamzehpoor, O. MacLean, M. Rajeswara Rao, Y. Chen, L. Besteiro, D. Dettmann, L. Ferrari, F. Frezza *et al.*, Synthesis of mesoscale ordered two-dimensional π-conjugated polymers with semiconducting properties, Nat. Mater. **19**, 874 (2020).

[23] Y. Zhou and F. Liu, Realization of an antiferromagnetic superatomic graphene: Dirac Mott insulator and circular dichroism Hall effect, Nano Lett. **21**, 230 (2021).

[24] See Supplemental Material at http://link.aps.org/supplemental/10.1103/PhysRevB.108.195429 for computational details of DFT, AIMD, *GW*, and BSE calculations.

[25] G. Kresse and J. Furthmüller, Efficiency of *ab-initio* total energy calculations for metals and semiconductors using a plane-wave basis set, Comput. Mater. Sci. **6**, 15 (1996).

[26] G. Kresse and J. Hafner, *Ab initio* molecular dynamics for open-shell transition metals, Phys. Rev. B **48**, 13115 (1993).

[27] J. P. Perdew, K. Burke, and M. Ernzerhof, Generalized gradient approximation made simple, Phys. Rev. Lett. **77**, 3865 (1996).

[28] G. Pizzi, V. Vitale, R. Arita, S. Blügel, F. Freimuth, G. Géranton, M. Gibertini, D. Gresch, C. Johnson, T. Koretsune *et al.*, Wannier90 as a community code: New features and applications, J. Phys.: Condens. Matter **32**, 165902 (2020).

[29] J. Bardeen and W. Shockley, Deformation potentials and mobilities in non-polar crystals, Phys. Rev. **80**, 72 (1950).

[30] J. Deslippe, G. Samsonidze, D. A. Strubbe, M. Jain, M. L. Cohen, and S. G. Louie, BerkeleyGW: A massively parallel computer package for the calculation of the quasiparticle and optical properties of materials and nanostructures, Comput. Phys. Commun. **183**, 1269 (2012).

[31] P. Giannozzi, S. Baroni, N. Bonini, M. Calandra, R. Car, C. Cavazzoni, D. Ceresoli, G. L. Chiarotti, M. Cococcioni, I. Dabo *et al.*, QUANTUM ESPRESSO: A modular and open-source software project for quantum simulations of materials, J. Phys.: Condens. Matter **21**, 395502 (2009).

[32] M. J. van Setten, M. Giantomassi, E. Bousquet, M. J. Verstraete, D. R. Hamann, X. Gonze, and G.-M. Rignanese, The PseudoDojo: Training and grading a 85 element optimized norm-conserving pseudopotential table, Comput. Phys. Commun. **226**, 39 (2018).

[33] S. Ismail-Beigi, Truncation of periodic image interactions for confined systems, Phys. Rev. B **73**, 233103 (2006).

[34] H. C. Andersen, Molecular dynamics simulations at constant pressure and/or temperature, J. Chem. Phys. **72**, 2384 (1980).

[35] M. P. Levendorf, C.-J. Kim, L. Brown, P. Y. Huang, R. W. Havener, D. A. Muller, and J. Park, Graphene and boron nitride lateral heterostructures for atomically thin circuitry, Nature (London) **488**, 627 (2012).

[36] Z. Liu, L. Ma, G. Shi, W. Zhou, Y. Gong, S. Lei, X. Yang, J. Zhang, J. Yu, K. P. Hackenberg *et al.*, In-plane heterostructures of graphene and hexagonal boron nitride with controlled domain sizes, Nat. Nanotechnol. **8**, 119 (2013).

[37] J. Thomas, J. Bradford, T. S. Cheng, A. Summerfield, J. Wrigley, C. J. Mellor, A. N. Khlobystov, C. T. Foxon, L. Eaves, S. V. Novikov *et al.*, Step-flow growth of graphene-boron nitride lateral heterostructures by molecular beam epitaxy, 2D Mater. **7**, 035014 (2020).

[38] J. Qiao, X. Kong, Z.-X. Hu, F. Yang, and W. Ji, High-mobility transport anisotropy and linear dichroism in few-layer black phosphorus, Nat. Commun. **5**, 4475 (2014).

[39] X. Liu, X. Ma, H. Gao, X. Zhang, H. Ai, W. Li, and M. Zhao, Valley-selective circular dichroism and high carrier mobility of graphene-like BC_6N, Nanoscale **10**, 13179 (2018).

[40] W. Feng, Y. Yao, W. Zhu, J. Zhou, W. Yao, and D. Xiao, Intrinsic spin Hall effect in monolayers of group-VI dichalcogenides: A first-principles study, Phys. Rev. B **86**, 165108 (2012).

[41] A. Chernikov, T. C. Berkelbach, H. M. Hill, A. Rigosi, Y. Li, B. Aslan, D. R. Reichman, M. S. Hybertsen, and T. F. Heinz, Exciton binding energy and nonhydrogenic Rydberg series in monolayer WS_2, Phys. Rev. Lett. **113**, 076802 (2014).

[42] M. S. Hybertsen and S. G. Louie, Electron correlation in semiconductors and insulators: Band gaps and quasiparticle energies, Phys. Rev. B **34**, 5390 (1986).

[43] M. Rohlfing and S. G. Louie, Electron-hole excitations and optical spectra from first principles, Phys. Rev. B **62**, 4927 (2000).

[44] G. Sethi, Y. Zhou, L. Zhu, L. Yang, and F. Liu, Flat-band-enabled triplet excitonic insulator in a diatomic kagome lattice, Phys. Rev. Lett. **126**, 196403 (2021).

[45] P. T. Mahon, R. A. Muniz, and J. E. Sipe, Quantum interference control of localized carrier distributions in the Brillouin zone, Phys. Rev. B **100**, 075203 (2019).

[46] Y. Sun, N. C. Giebink, H. Kanno, B. Ma, M. E. Thompson, and S. R. Forrest, Management of singlet and triplet excitons for efficient white organic light-emitting devices, Nature (London) **440**, 908 (2006).

[47] Z. Shuai, D. Beljonne, R. Silbey, and J. L. Brédas, Singlet and triplet exciton formation rates in conjugated polymer light-emitting diodes, Phys. Rev. Lett. **84**, 131 (2000).